Modelling of cutting forces and researching calibration method in helical milling

Shang, S., Qin, X. D., Li, J. H., Li, S. P., Li, H., Huang, T., Jin, Y., & Sun, D. (2018). Modelling of cutting forces and researching calibration method in helical milling. *International Journal of Advanced Manufacturing Technology*, *94*(5-8), 2949-2960. https://doi.org/10.1007/s00170-017-1117-0

Published in:
International Journal of Advanced Manufacturing Technology

Document Version:
Peer reviewed version

Noname manuscript No.
(will be inserted by the editor)

Modelling of cutting forces and researching calibration method in helical milling

S Shang · XD Qin* · JH Li · SP Li · H Li · T.Huang · Y Jin · D Sun

Received: date / Accepted: date

Abstract Helical milling is a high efficiency, high quality hole-making technology, which enjoys very good usage prospects for the aeronautical and aerospace industry. In the helical milling process, the chip thickness is highly variable along the cutting edges and during the tool revolution due to the special cutting trajectory. The aim of this study is to develop a cutting force model and build a new calibration method of cutting force coefficients for helical milling. First, the tool motion of helical milling and the geometry of the chip are analyzed, and then the cutting force model is established. After that the calibration method of cutting force coefficients is built. In the end, a series of cutting experiments were conducted to validate the cutting force model and the calibration method. With this model, it is possible to analyze cutting forces and optimize the cutting parameters, and then get a better quality of hole-making.

Keywords Helical milling · Cutting forces · Calibration method · Cutting coefficients

1 Introduction

Hole-making is the most performed machining operation for assembly processes, and drilling is largely performed to machine boreholes for rivets or bolts, in the aeronautical and aerospace industries. The hole quality has critical requirements

S Shang, XD Qin*, SP Li, H Li , JH Li

Key Laboratory of Mechanism Theory and Equipment Design of Ministry of Education, Tianjin University, Tianjin 300072, China.
XD Qin E-mail: qxd@tju.edu.cn

T.Huang

School of Engineering, The University of Warwick, Coventry CV4 7AL, UK

Y Jin , D Sun

School of Mechanical and Aerospace Engineering, Queens University, Belfast, UK.

to ensure aviation safety. However, some materials which are widely used in the aeronautical and aerospace industry are difficult to drill, such as Titanium alloy and carbon fiber composite material [1,2]. So, some new hole making technologies were invented to cater to the demands of high quality boreholes in the aeronautical and aerospace industry. As one of the new hole machining technologies, helical milling offers many advantages compared to conventional drilling. For example, one tool can be used to produce different borehole geometries by changing the process parameters of helical milling. Another advantage is there is no need to change the tool when helical milling bores holes with different diameters, so it offers the possibility for a dynamic correction of the bore diameter during the drilling process. Other advantages of helical milling are lower process forces, better chip transportation and better cutting fluid conditions than conventional drilling [3]. Some research compared the helical milling with drilling in boreholes of different materials and found that helical milling is better than conventional drilling in cost savings, environmental protection, holes quality and process productivity [4–7]. Therefore, helical milling is a good application in boreholes for difficult-to-cut aeronautical materials.

The investigation on helical milling, that focus on surface topography and roughness [8,9], optimization of process [10,11], experimental study for cutting forces and machining quality [12], has achieved great development in recent years.

However, the cutting process of helical milling is very complex, and the cutting force modelling of helical milling is hard to build. But it is very important for analysis of the cutting process and optimization of the process to investigate cutting forces modelling of helical milling. In addition, the cutting forces modelling is the basis in which researchers analyze cutting temperature and machining stability in helical milling. In 2013, a novel modelling of cutting forces for helical milling process was established [13] based on traditional milling model of cutting force in milling [14]. However, the model can be improved as the change axial cutting depth is not considered. In 2014, tool was considered to be non-rigid in a novel cutting force modelling of helical milling. By using this modelling the regenerative chatter stability of helical milling was analyzed [15], but how to calibrate the coefficients of cutting force is considered in less detail in the paper. The cutting force modelling is made by semi-analytical approaches, and the coefficients is very important to the accuracy of the modelling, so it is necessary to research on the method of calibrating cutting force coefficients to give a more accurate model. Because the chip thickness of helical milling is highly variable during the tool revolution, it is not easy to calibrate the coefficients of cutting force like traditional milling. For example, in 2016, a dedicated workpiece and measurement of the cutting force coefficient of different cutting depths to calibrate the coefficients [16].

The helical milling chip geometry are so complicated that the cutting force coefficient calibration is difficult. Furthermore, the cutting force calibration method in helical milling lacks deep research. So,in this paper research works are focused on the following aspects: (1) rebuilding the cutting force model in helical milling and, (2) researching the new calibration tests method for helical milling. The paper is organized as follows: Sect. 2 describes the process and chip shape of helical milling. Sect. 3 presents cutting force modelling of helical milling. The calibration method of coefficients is introduced in Sect. 4. The experimental procedures are performed in Sect. 5. The cutting force simulation and experiment results are discussed in Sect. 6. Conclusions are finally made in Sect. 7.

2 Helical milling mechanism and cutting chip analysis

2.1 Helical milling mechanism

In helical milling the borehole is generated by a milling tool which executes a helical path into the workpiece, as shown in Fig.1. There are three movements in the helical milling hole-making process: the orbital rotation n_c, the movement in the axial direction v_z and the spindle rotation n. The superposition of the first two movements offers a helical course. The determine the bore diameter (radius)D_h (R_h) can be determined by eccentric distance e and the tool diameter (radius) D_t (R_t), see Eq. 1.

$$D_h = 2e + D_t \tag{1}$$

When the cutting forces were analyzed, three cutting parameters were used: the axial feed per orbital revolution a_p, the feed per tooth of tool center s_t and the spindle rotation n.
The motion of cutting edge in the $x-y$ plane is given by Eq. 2.

$$\begin{cases} x = e\cos(\frac{2\pi n_c t}{60}) + R_t\cos(\theta_0 + \frac{2\pi n t}{60}) \\ y = e\sin(\frac{2\pi n_c t}{60}) + R_t\sin(\theta_0 + \frac{2\pi n t}{60}) \end{cases} \tag{2}$$

The feed of conventional milling is straight line motion. However the feed of helical milling is circular motion. In previous papers the period of feed was the time per revolution of cutting tool. Because the spindle speed is much higher than the orbital rotates, the cutting force error is small in one period feed. But the error cannot be omitted when the cutting force modelling of helical milling is built in the time-domain. Because the simulation time requires a few periods of orbital rotation, the cumulative error per period feed is large. The period of feed T is the interval when the distance of a cutting edge to the center of hole changes from R_h to next R_h, see Fig. 1. T and the feed f_T given is given by Eq. 3 and Eq. 4. The relationship of the per tooth feed s_t with f_T is given by Eq. 5, and the period of the feed per tooth T_s is given by Eq. 6. N is the number of tooth.

$$T = \frac{60}{n - n_c} \tag{3}$$

$$f_T = \frac{2\pi e n_c T}{60} = \frac{2\pi e n_c}{n - n_c} \tag{4}$$

$$s_t = \frac{f_T}{N} = \frac{2\pi e n_c}{N(n - n_c)} \tag{5}$$

$$T_s = \frac{T}{N} = \frac{60}{N(n - n_c)} \tag{6}$$

There are two coordinate systems used in the modelling of cutting forces for helical milling, see Fig. 2. One is the workpiece coordinate system. Its a fixed coordinate system and has an origin of coordinates O_w. The other is the tool coordinate system. It is a moving coordinate system that it is origin of coordinates O_c goes around the O_w. Besides, the coordinate axis y_c always points to the direction of the tool motion. The note ϕ is the tool rotated angle in workpiece coordinate system. The note θ is the tooth rotated angle in the tool coordinate system.

2.2 Instantaneous cutting chip analysis in helical milling

The chip geometry is an important parameter for calculating the cutting force. Therefore, it is necessary to analyze the chip geometries.
The front cutting edge and the side cutting edge of cutting-tool take part in the helical milling process simultaneously, so the chip has two components, see Fig. 3. The one is the cutting volume for the front V_f, and the other is the cutting volume for the side cutting V_p. Because the spindle speed n is much bigger than the orbital rotation n_c, the chip can be considered as two kinds of production from the conventional drilling and milling [13]. The cutting of the front edge was approximately considered as the conventional drilling. The thickness of chip h for the process of front cutting is a constant that is equal to a_t, see Eq. 7, and axial cutting depth b is approximate equal to R_t.

$$a_t = \frac{s_t a_p}{\pi(D_h - D_t)} \tag{7}$$

The cutting process of the side edge like the conventional milling and the thickness of chip h varies with the tooth rotated angle θ, see Fig. 3. The tooth trajectory is considered circular (cycloid effect neglected), according to Segonds et al. [18]. But axial cutting depth b is different to the milling, because axial cutting depth b changes with the position of the side cutting edge [15,19]. As shown in Fig. 3, O_c is the current tool center location, and P_c is the position of nose of tool. The tooth machined point P_c many times in the previous tool orbital period, and the point O_k is the tool center location when the last time the tool orbital period tooth machined point P_c, so P_cO_k equals R_t. The θ_k is the angle between O_wO_c with O_wO_k. The side edge axial cutting depth b equaling the difference of altitude following z between two tool locations O_c and O_k. The side edge axial cutting depth b is defined according to the relative angular position θ_k:

$$b(\theta_k) = a_p - \frac{a_p}{2\pi}\theta_k \tag{8}$$

According to the law of cosines the length of the P_cO_w can be found:

$$P_cO_w^2 = P_cO_c^2 + O_cO_w^2 - 2P_cO_c \times O_cO_w \cos(\pi - \theta) = R_t^2 + e^2 - 2R_te\cos(\pi - \theta) \tag{9}$$

and

$$P_cO_c^2 = P_cO_w^2 + O_cO_w^2 - 2P_cO_w \times O_cO_w \cos(\frac{\theta}{2}) = P_cO_w^2 + e^2 - 2P_cO_w \times e\cos(\frac{\theta_k}{2}) \tag{10}$$

Based on the Eq. 9 and Eq. 10 the θ_k is defined according to the θ:

$$\theta_k = 2arc\cos(\frac{e - R_t\cos(\theta)}{\sqrt{e^2 + R_t^2 - 2R_te\cos(\theta)}}) \tag{11}$$

According to the Eq. 11 the side edge axial cutting depth b is defined according to the tooth rotated angle θ:

$$b(\theta) = a_p - \frac{a_p}{\pi}arc\cos(\frac{e - R_t\cos(\theta)}{\sqrt{e^2 + R_t^2 - 2R_te\cos(\theta)}}) \tag{12}$$

3 Cutting force modelling of helical milling

As the available axial depth per orbital revolution in helical milling is very small, the lag angle caused by the helix angle is omitted since it is negligible. The radial F_r^i, tangential F_t^i, and axial F_a^i cutting forces of side cutting edge for the i tooth are given by Eq. 13. The tooth is equally distributed, so all the teeth rotated angles can be calculated as long as one teeth rotated angle is known. The superscript i of θ^i represents for the number of tooth. The radial and tangential components of different tooth are different for different , but the equation has no different.

$$\begin{cases} F_{Pr}^i = k_{Pr}b(\theta^i)h(\theta^i) + k_{Pre}b(\theta^i) \\ F_{Pt}^i = k_{Pt}b(\theta^i)h(\theta^i) + k_{Pte}b(\theta^i) \\ F_{Pa}^i = k_{Pa}b(\theta^i)h(\theta^i) + k_{Pae}b(\theta^i) \end{cases} \tag{13}$$

Equation 13 has two kinds of coefficients: one is associated with cutting (or s-hearing) and includes the chips thickness dependence, represented by k_{Pr}, k_{Pt} , k_{Pa}; and the other is the rubbing(or plowing) term, which is independent of chip thickness (denoted by the e subscript extension), represented by k_{Pre}, k_{Pte}, k_{Pae}. The six coefficients can be obtained via average cutting force linear regression. These average cutting force can be measured by the dynamometer over a range of feed per tooth. $h(\theta^i)$ is the immersion dependent chip thickness cut by tooth i. The engagement conditions lead to the prediction of varying chip thickness at each tool location as it rotates and the without deformed chip thickness at a certain location on the cutting edge can be estimated as Eq. 14

$$\begin{cases} h(\theta^i) = s_t \sin(\theta^i), 0 \le \theta^i \le 180^\circ \\ h(\theta^i) = 0, 180^\circ < \theta^i < 360^\circ \end{cases} \tag{14}$$

Because the chip thickness of front cutting edge is constant that equal to a_p, and every tooth work togetherthe resultant radial force of front cutting edge is zero. The front cutting edges only contribute to the axial cutting force, see Eq. 15

$$F_{Fa}^i = k_{Fa}R_t a_t + k_{Fae}R_t \tag{15}$$

The total force is given by Eq. 16

$$\begin{cases} F_r = \sum_{i=1}^{N} g(\theta^i)[k_{Pr}b(\theta^i)h(\theta^i) + k_{Pre}b(\theta^i)] \\ F_t = \sum_{i=1}^{N} g(\theta^i)[k_{Pt}b(\theta^i)h(\theta^i) + k_{Pte}b(\theta^i)] \\ F_a = \sum_{i=1}^{N} g(\theta^i)[k_{Pa}b(\theta^i)h(\theta^i) + k_{Pae}b(\theta^i)] + N[k_{Fa}R_t a_t + F_{Fae}R_t] \end{cases} \tag{16}$$

Where $g(\theta^i)$ is used to define whether the tooth i is cut or not; $g(\theta^i) = 1$ as the tooth is cutting, and $g(\theta^i) = 0$ when the tooth is out of cut.
The forces of side cutting edge are finally evaluated and measured in the workpiece coordinate system, and thus by transformation, the radial force F_r, the tangential force F_t and the axial force F_a are the expressed in the tool coordinate system as:

$$\begin{cases} F_{cx} = -\cos(\theta)F_r + \sin(\theta)F_t \\ F_{cy} = -\sin(\theta)F_r - \cos(\theta)F_t \\ F_{cz} = F_a \end{cases} \tag{17}$$

Then the forces F_{cx}, F_{cy} and F_{cz} are expressed in the workpiece coordinate system as:

$$\begin{cases} F_{wx} = \cos(\phi)F_{cx} - \sin(\phi)F_{cy} \\ F_{wy} = \sin(\phi)F_{cx} + \cos(\phi)F_{cy} \\ F_{wz} = F_{cz} \end{cases} \tag{18}$$

According to the Eq. 17 and Eq. 18 cutting force in workpiece coordinate system is defined according to the radial force F_r, the tangential force F_t and the axial force F_a:

$$\begin{cases} F_{wx} = (-\cos\phi\cos\theta + \sin\phi\sin\theta)F_r + (\cos\phi\sin\theta + \sin\phi\cos\theta)F_t \\ F_{wy} = (-\sin\phi\cos\theta + \sin\phi\sin\theta)F_r + (\sin\phi\sin\theta + \sin\phi\cos\theta)F_t \\ F_{wz} = F_a \end{cases} \tag{19}$$

4 Calibration tests method of cutting force coefficients

4.1 The side edge cutting force coefficients calibrated method in helical

There are eight coefficients in the cutting force modelling. The cutting of side edges is like the traditional milling. So the calibration of six side edge coefficient k_{Pr}, k_{Pt}, k_{Pa}, k_{Pre}, k_{Pte} and k_{Pae} can be conducted via slot milling experiments and linear regression using the average cutting forces [17], which can be measured by the dynamometer over a range of feed per tooth values. As shown in Fig. 4, these tests are carried out by prescribing a known feed per tooth and axial depth and measuring the x (feed), y, and z (axial) direction cutting force components in the dynamometers fixed coordinate frame. According to the traditional milling cutting force model [17], the radial F_{mr}, tangential F_{mt}, and axial F_{ma} cutting forces of slot milling are defined as:

$$\begin{cases} F_{mr} = k_{Pr}bh(\theta) + k_{Pre}b \\ F_{mt} = k_{Pt}bh(\theta) + k_{Pte}b \\ F_{ma} = k_{Pa}bh(\theta) + k_{Pae}b \end{cases} \tag{20}$$

By transformation the cutting force in workpiece coordinate system is defined according to the radial force F_{mr}, the tangential force F_{mt} and the axial force F_{ma}:

$$\begin{cases} F_{wx} = k_{Pt}bs_t\sin(\theta)\cos(\theta) + k_{Pte}b\cos(\theta) + k_{Pr}bs_t\sin^2(\theta) + k_{Pre}b\sin(\theta) \\ F_{wy} = k_{Pt}bs_t\sin^2(\theta) + k_{Pte}b\sin(\theta) - k_{Pr}bs_t\sin(\theta)\cos(\theta) - k_{Pre}b\cos(\theta) \\ F_{wz} = -k_{Pa}bs_t\sin(\theta) - k_{Pae}b \end{cases} \tag{21}$$

The mean force per revolution is determined by Eq 22. Because the integration limits are set between the start and exit angles, the switching function $g(\theta)$ is always equal to one. Meanwhile, the summation is incorporated by the multiplication of the integral by N, as shown in Eq. 16. The mean force equation is rewritten by Eq. 23.

$$\overline{F} = \frac{1}{2\pi}\int_{\theta_s}^{\theta_e} F d\theta \tag{22}$$

$$\begin{cases} \overline{F}_{wx} = \frac{N}{2\pi}\int_{\theta_s}^{\theta_e}(k_{Pt}bs_t\sin(\theta)\cos(\theta) + k_{Pte}b\cos(\theta) + k_{Pr}bs_t\sin^2(\theta) + k_{Pre}b\sin(\theta))d\theta \\ \overline{F}_{wy} = \frac{N}{2\pi}\int_{\theta_s}^{\theta_e}(k_{Pt}bs_t\sin(\theta)^2 + k_{Pte}b\sin(\theta) - k_{Pr}bs_t\sin(\theta)\cos(\theta) - k_{Pre}b\cos(\theta))d\theta \\ \overline{F}_{wz} = \frac{N}{2\pi}\int_{\theta_s}^{\theta_e}(k_{Pa}bs_t\sin(\theta) + k_{Pae}b)d\theta \end{cases} \tag{23}$$

when the θ_s equal 0 and the θ_e equal π, the Eq. 23 simplify to

$$\begin{cases} \overline{F}_{wx} = \frac{Nbk_{Pr}}{4}s_t + \frac{Nbk_{Pre}}{\pi} \\ \overline{F}_{wy} = \frac{Nbk_{Pt}}{4}s_t + \frac{Nbk_{Pte}}{\pi} \\ \overline{F}_{wz} = -\frac{Nbk_{Pa}}{\pi}s_t - \frac{Nbk_{Pae}}{2} \end{cases} \tag{24}$$

If we consider s_t is variate and other parameters are constant, then Eq. 24 are linear equation with an unknown number. The slopes and intercepts of the linear equations can be obtained by milling tests linear regression results under different s_t. In the x direction, for example, the slope is $\frac{Nbk_{Pr}}{4}$ and the intercept is $\frac{Nbk_{Pre}}{\pi}$. The six unknown cutting force coefficients: k_{Pr}, k_{Pre}, k_{Pt}, kP_{te}, k_{Pa} and k_{Pae} will be obtained with above method.

4.2 The front edge cutting force coefficients calibrated method in helical

Carrying out helical milling cutting tests obtains the coefficients: k_{Fa} and k_{Fae}. To distinguish the cutting force of z direction in the slot milling, we use the F_{hz} for the cutting force of z direction in helical milling. From Eq. 16 the F_{hz} can be written as:

$$F_{hz} = -\sum_{i=1}^{N} g(\theta^i)[k_{Pa}b(\theta^i)h(\theta^i) + k_{Pae}b(\theta^i)] - N[k_{Fa}R_ta_t + F_{Fae}R_t] \tag{25}$$

Because the function $b(\theta)$ is complicated, it is fitted by 4-order polynomial fitting, see Eq. 26. Those unknown coefficients p_1 to p_5 will be change as the cutting parameters change. When a_p equals 0.3mm, D_h equal 10mm and D_t equal 6mm, the function $b(\theta)$ and $b_p(\theta)$ are simulated from 0 to 180 degree, see Fig. 5. The root mean squared error between the function $b(\theta)$ and $b_p(\theta)$ is $8.89 * 10^{-07}$, suggesting that 4-order polynomial has high goodness-of-fit with the function $b(\theta)$.

$$b_p(\theta) = p_1\theta^4 + p_2\theta^3 + p_3\theta^2 + p_4\theta + p_5 \tag{26}$$

The mean force per revolution is determined by $\overline{F} = \frac{N}{2\pi}\int_{\theta_s}^{\theta_e} Fd\theta$, and considers the force that come from different teeth. The $\overline{F}_{hz}$ can be written as Eq. 27.

$$\overline{F}_{hz} = -\frac{N}{2\pi}\int_{\theta_s}^{\theta_e}[k_{Pa}s_tb_p(\theta^i)\sin(\theta^i) + k_{Pae}b_p(\theta^i)]d\theta - [\frac{Nk_{Fa}R_ta_p}{\pi(D_H - D_T)}s_t + Nk_{Fae}R_t] \tag{27}$$

Because the $\theta_S \approx 0$ and the $\theta_e \approx \pi$ and Eq. 28 simplify to

$$\begin{aligned} \overline{F}_{hz} = &-[\tfrac{Nk_{Pa}}{2\pi}(5.92p_1 + 24.31p_2 + 15.74p_3 + 6.28p_4 + 2p_5)s_t \\ &+ \tfrac{Nk_{Pae}}{2\pi}(61.2p_1 + 24.35p_2 + 10.34p_3 + 4.93p_4 + 3.14p_5)] \\ &-[\tfrac{Nk_{Fa}R_ta_p}{\pi(D_H - D_T)}s_t + Nk_{Fae}R_t] \end{aligned} \tag{28}$$

Then through the merger of similar items.The slope and the intercept can be obtained. If the helical milling parameters are confirmed, the coefficients: k_{Fa} and k_{Fae} are the only unknown parameters. So, the coefficient k_{Fa} and k_{Fae} can be obtain by doing the cutting tests at different s_t and dealing with the experimental data using the method of linear regression.

The axial cutting depth b is constant in traditional milling. b_e is the value of axial cutting depth b in an experiment and b_c is the value of axial cutting depth b to calibrate cutting force coefficients. The cutting force coefficients will change when cutting force coefficients are calibrated in different axial cutting depth b. If b_c equal b_e, the cutting force model will have a better simulation result for experiment cutting force and the difference between b_c and b_e is bigger, the error of simulation is bigger [17]. However, the side edge axial cutting depth b is variable in helical milling, so the six side edge coefficients k_{Pr}, k_{Pt}, k_{Pa}, k_{Pre}, k_{Pte} and k_{Pae} are measured in the side edge axial mean cutting depth $\overline{b}$ to decrease the difference between b_c and b_e. The side edge axial mean cutting depth $\overline{b}$ is determined by Eq. 12 and Eq. 29.

$$\overline{b} = \frac{1}{\theta_e - \theta_s} \int_{\theta_s}^{\theta_e} b(\theta) d\theta \tag{29}$$

5 Experimental procedures

In order to verify the cutting force modelling, a series of helical milling operations were performed on DMC75Vlinear 5-axis highspeed machining center. A Kistler three-direction stationary dynamometer (9257) with supporting Kistler charge amplifier (type 5070) was used, and data acquisition board and Kistler software were deployed for the horizontal and vertical directions cutting force measurements, see Fig. 6.

Holes of 10 mm in diameter, $D_h = 10$ mm, are produced with a solid carbide end mill with see Fig. 6b and the parameters of cutting tool see Table 1. The workpiece material used in the machining experiment was titanium alloy (Ti6Al4V) with 10 mm thickness, length of 250 mm, and width of 120 mm, and the basic physical properties are summarized in Table 2 and 3. The cutting conditions of helical milling and slot milling are given as Table 4. The one purpose of these experiments is to identify the cutting coefficient in the cutting depth b and a_p. The other purpose is to analyze the accuracy of cutting force model models which use the cutting coefficient measured in the cutting depth $\overline{b}$ and a_p.

To analyze the influence of a_p on cutting force, some other helical milling experiments have been done, and the cutting conditions are show in Table 5. This experiments are to analyze the influence of a_p on cutting force. The cutting force signal was analyzed by the software DYNOWARE, with the cutting forces of slotting and the cutting forces of helical milling shown in Fig 7 and Fig 8. We can get the mean cutting force by using the software DYNOWARE, and then the cutting force coefficients can be obtained by using the method in the section 4. The helical milling cutting force in x and y direction are basically identical, but the phase difference is 90 degree between them. So a mean cutting force is defined in x and y directions $\overline{F}_{hxy}$ and in z direction $\overline{F}_{hz}$ to compare between simulations

and experimental measurements. The $\overline{F}_{hxy}$ is defined by Eq. 30.

$$\overline{F}_{hxy} = \frac{F_{ctx} + F_{cty} + |F_{thx} + F_{thy}|}{4} \tag{30}$$

Because the cutting force signals in x and y directions like sine function or cosine function, see Fig. 8, crest cutting force F_{ctx}, F_{cty} and trough cutting force F_{thx}, F_{thy} means the peaks and the valleys of cutting force signals in x and y direction, respectively. The period and amplitude are important parameters for sine function or cosine function. The crest cutting force and trough cutting force are easy to measure and those force are also the important parameters to show the amplitude in x and y directions. So Eq. 30 can be used to verify the accuracy of the cutting force model and is employed to compare simulations and measurements. The value of crest cutting force and trough cutting force are measured by Kistler dynamometer and read by Kistler software directly.

6 Results and discussion

6.1 The accuracy analysis of cutting force model

This part is to analysis the accuracy of cutting force model that was calibrated in different cutting depth b. The error values are calculated by Eq. 31. According to the parameters of Table 4, the cutting force coefficients under different cutting depth can be obtained, see Table 6. The cutting force coefficients $k_{0.188}$ were obtained at $b = 0.188$ mm, and the cutting force coefficients $k_{0.3}$ was obtained at $b = 0.3$ mm. According to the model of cutting force and the cutting force coefficient $k_{0.188}$ and $k_{0.3}$ the cutting force simulation has been implemented using MATLAB. Experimental results are closely matched with the theoretical simulation results, see Fig 9. The experiment and simulation results are listed in Table 7.

$$\begin{cases} R_{hxy} = \frac{\overline{F}_{hexy} - \overline{F}_{hxy}}{\overline{F}_{hexy}} \\ R_{hz} = \frac{\overline{F}_{hez} - \overline{F}_{hz}}{\overline{F}_{hez}} \end{cases} \tag{31}$$

The error between simulation and experimental results are shown in Table 8. According to Table 8, the cutting force mean error in x and y direction R_{hxy} is 4.08% at the coefficients $k_{0.188}$ and the mean error R_{hxy} is 15.72% at the coefficients $k_{0.3}$. The cutting force mean error in z direction R_{hz} are small at both the coefficients $k_{0.188}$ and the coefficients $k_{0.3}$, but at the coefficients $k_{0.188}$ the cutting force model has higher accuracy to predict the cutting force oscillation amplitude in z direction. The reason why two mean error R_{hz} are small is that they are calibrated by the same cutting parameter, so the experimental resultant forces from side edge and front edge in z direction are the same. The coefficients k_{Pa} and k_{Pae} of $k_{0.3}$ are smaller than the coefficients k_{Pa} and k_{Pae} of $k_{0.188}$. However the coefficients k_{Fa} and k_{Fae} of $k_{0.3}$ are larger than the coefficients k_{Fa} and k_{Fae} of $k_{0.188}$ so that the simulation resultant forces are the same. But the cutting forces of the side edge in z direction are small if the coefficients k_{Pa} and k_{Pae} are small. Besides, this cutting force is fluctuant. The two reasons result in that the simulation cutting force oscillation amplitude in z direction are smaller

at the coefficient $k_{0.3}$. These results show that the cutting force model which is calibrated in mean cutting depth $\bar{b}$ has a higher accuracy.

6.2 The accuracy analysis of cutting force model in different a_p

In this part, the cutting force model at the coefficients $k_{0.188}$ is used to predict the cutting force of helical milling in different a_p. According to the parameters of Table 5, the experiments and the simulations have been done. The results and error are listed in Table 9. The Table 9 shows that the simulation cutting forces will be less than the experiments cutting forces when a_p is less than 0.3mm/rev. On the other hand, the simulation cutting forces are larger than the experiments cutting force when the a_p is larger than 0.3mm/rev. The reason is that the cutting force coefficients will decrease in general, when the cutting depth b increases [13]. At the same cutting parameters, the cutting forces will be smaller when the cutting force coefficients are smaller. So the cutting force coefficients $k_{0.188}$ are too small when the cutting force model predict the cutting force of helical milling that the a_p less than 0.3mm/rev. On the contrary, the cutting force coefficients $k_{0.188}$ are too large when the a_p are large than the 0.3mm/rev.
The high error values are caused by the large difference between b_c and b_e [17]. So the results of experiments and simulations No.21 to No.23 show that the cutting force model which is calibrated for a axial depth of cut per revolution a_p, has worse accuracy to predict the cutting force of helical milling when the a_p become small. Besides the error increase very fast with the a_p decrease. So the cutting force coefficients which are calibrated for a a_p are not fit to predict the cutting force of helical milling when the a_p becomes too small. Based on Table 9 the cutting forces error R_{hxy} are larger than the R_{hz}. The reason is that the cutting depth of front cutting edge is smaller than the side cutting edge mean cutting depth $\bar{b}$ and the cutting depth changes less with the change of a_p. So, the cutting depth of front edge for calibration are closer to corresponding actual cutting depth than the cutting depth of side edge for calibration when the a_p has changed.

7 Conclusions

This study focuses on modelling of cutting forces in helical milling and researching its coefficient calibration method. Considering the chip geometry characteristic of helical milling, the new cutting forces model and calibration method were set up, and the correctness of the model was proved by experiments. The following conclusions can be drawn from this work:
1. The side edge cutting depth in helical milling nonlinearly change with the tooth rotated angle θ. The side edge mean cutting depth $\bar{b}$ in helical milling can be decided by three parameters: the axial feed per orbital revolution a_p, the eccentric distance e and the tool radius R_t. The cutting depth which is selected to calibrated cutting force coefficients has considerable influence on the accuracy of cutting force model in helical milling. When the cutting parameters of helical milling are certain, selecting the mean cutting depth θ of helical milling to calibrate the side edge cutting force coefficients is very helpful to improve the accuracy of the cutting force model.

2. Using the new cutting force coefficients calibrated method the specialized workpieces are needless. The side edge cutting force coefficients can be calibrated by slotting milling experiments and then the front edge cutting force coefficients can be calibrated by helical milling experiments. Besides, there is no need to calibrate the side edge cutting force coefficients at different cutting depth b. For this reason, the experiment quantity is reduced greatly.
3. Because of the size effect, when the cutting parameters of helical milling are certain, the simulation cutting forces of the cutting force model will be smaller when the cutting force coefficients is calibrated at a cutting depth b which is larger than the mean cutting depth θ. On the contrary, the simulation cutting forces of the cutting force model will be larger when the cutting force coefficients is calibrated at a cutting depth b which is less than the mean cutting depth θ.
4. Because of the size effect, the cutting force coefficients has its range of application. If cutting force coefficients is calibrated for an axial depth of cut per revolution a_p of helical milling, the error between the simulation cutting forces of the cutting force model and experiment cutting forces increase very fast with the a_p decrease. So the cutting force model has better accuracy when the a_p does not change or changes a bit bigger.
In summary, compared to the previous cutting force modelthe new cutting force model can better predict the change of cutting force in helical milling process. The new calibration method of cutting force coefficients is more convenient to calibrate the cutting force coefficients. These research results can be used to optimize the cutting conditions and analyze helical milling process.

Acknowledgements The authors are grateful for funding supports by National Natural Science Foundation of China (Nos 51605326 and 51420105007), Science and the Natural Science Foundation of Tianjin (Nos 16JCZDJC38300 and 16PTSYJC00150).

References

1. D1 Kim, Usage of PCD tool in drilling of titanium/graphite hybrid composite laminate, International Journal of Machining and Machinability of Materials, 13(2/3), 276-288 (2016).
2. Xu J, Mkaddem A, Mansori M E, Recent advances in drilling hybrid FRP/Ti composite: A state-of-the-art review, Composite Structures, 135(1), 316-338 (2016).
3. Zitoune R, Krishnaraj V, Collombet F, SL Roux, Experimental and numerical analysis on drilling of carbon fibre reinforced plastic and aluminium stacks, Composite Structures, 146, 148-158 (2016).
4. Qing Zhao, Xuda Qin, Chunhui Ji, Yonghang Li, Dan Sun, Yan Jin, Tool life and hole surface integrity studies for hole-making of Ti6Al4V alloy, The International Journal of Advanced Manufacturing Technology, 79(5-8), 1017-1026 (2015).
5. RBD Pereira, LC Brandao, APD Paiva, JR Ferreira, JP Davim, A REVIEW OF HELICAL MILLING PROCESS, International Journal of Machine Tools and Manufacture, 120, 27-48 (2017).
6. Denkena B, Boehnke D, Dege J H, Helical milling of CFRP-titanium layer compounds, CIRP Journal of manufacturing Science and Technology, 1(2), 64-69 (2008).
7. Iyer R, Koshy P, Ng E, Helical milling: an enabling technology for hard machining precision holes in AISI D2 tool steel, International Journal of Machine Tools and Manufacture, 47(2), 205-210 (2007).
8. Brinksmeier E, Fangmann S, Rentsch R, Drilling of composites and resulting surface integrity, CIRP Annals-Manufacturing Technology, 60(1), 57-60 (2011).
9. Zhou L, Ke Y, Dong H, Chen Z, Gao K, Hole diameter variation and roundness in dry helical milling of CFRP/Ti stacks, The International Journal of Advanced Manufacturing Technology, 87(1-4), 811-824 (2016).

10. Sadek A, Meshreki M, Attia M H, Characterization and optimization of helical milling of woven carbon fiber reinforced epoxy laminates, CIRP Annals-Manufacturing Technology, 61(1), 123-126 (2012).
11. M Wang, N Liu, XU Yingxiang, D Liu, Q Jiang, Experimental Study on Milling Force and Hole Milling Quality of Helical Hole Milling for Carbon Fiber Reinforced Plastics, Machine Tool and Hydraulics,19, (2015).
12. Li Z, Liu Q, Surface topography and roughness in hole-making by helical milling, The International Journal of Advanced Manufacturing Technology, 66(9-12), 1415-1425 (2013).
13. Wang H, Qin X, Ren C, et al, Prediction of cutting forces in helical milling process, The International Journal of Advanced Manufacturing Technology, 58(9-12), 849-859 (2012).
14. Altintas Y, Spence A, Tlusty J, End Milling Force Algorithms for CAD Systems, CIRP Annals - Manufacturing Technology, 40(1), 31-34 (1991).
15. Li Z, Liu Q, Ming X, Wang X, Dong Y, Cutting force prediction and analytical solution of regenerative chatter stability for helical milling operation, The International Journal of Advanced Manufacturing Technology, 73(1), 433-442 (2014).
16. P.A. Rey, J. LeDref, J. Senatore, Y Landon, Modelling of cutting forces in orbital drilling of titanium alloy Ti-6Al-4V, International Journal of Machine Tools and Manufacture,106, 75-88 (2016).
17. Altintas Y, Manufacturing Automation: Metal Cutting Mechanics Machine Tool Vibrations and CNC Design, 35-47. Cambridge University Press, UK (2012).
18. Segonds S, Landon Y, Monies F, Pierre L, Method for rapid characterisation of cutting forces in end milling considering runout, International Journal of Machining and Machinability of Materials, 1(1), 45-61 (2006).
19. Tian Y, Liu Y, Wang F, Jing XB, Zhang DW, Liu XP, Modeling and analyses of helical milling process, The International Journal of Advanced Manufacturing Technology,90(1-4), 1003-1022 (2017).

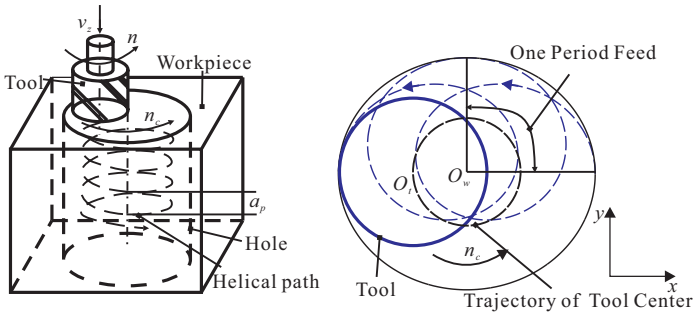

Fig. 1 Helical milling process

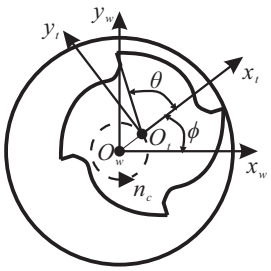

Fig. 2 Workpiece coordinate system and tool coordinate system

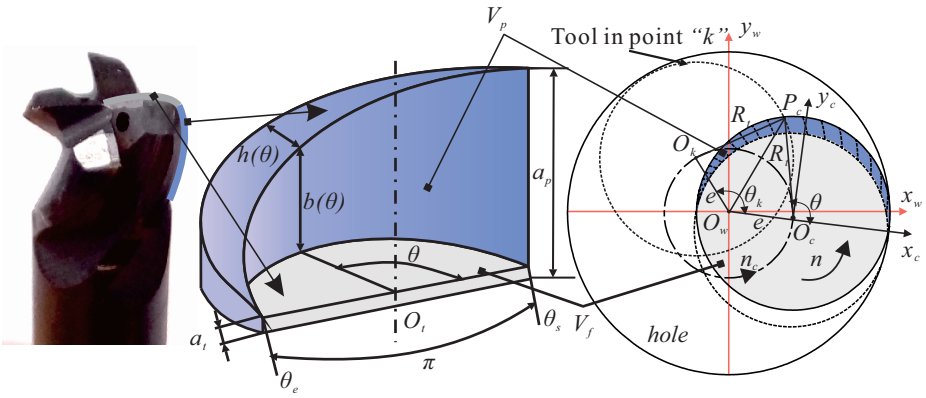

Fig. 3 The chip shape of different cutting edges

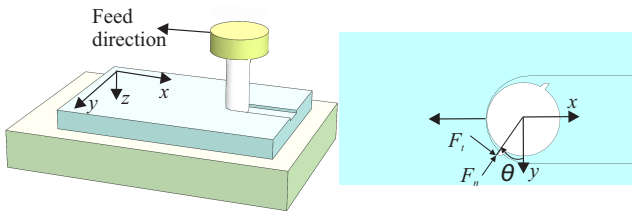

Fig. 4 Slot milling experiments

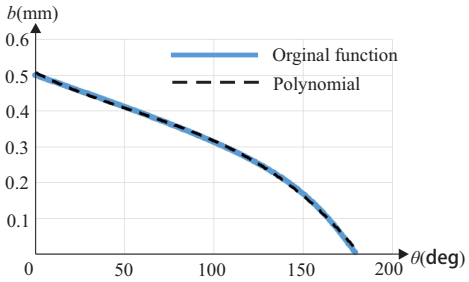

Fig. 5 The simulation curve of function $b(\theta)$ and $b_p(\theta)$

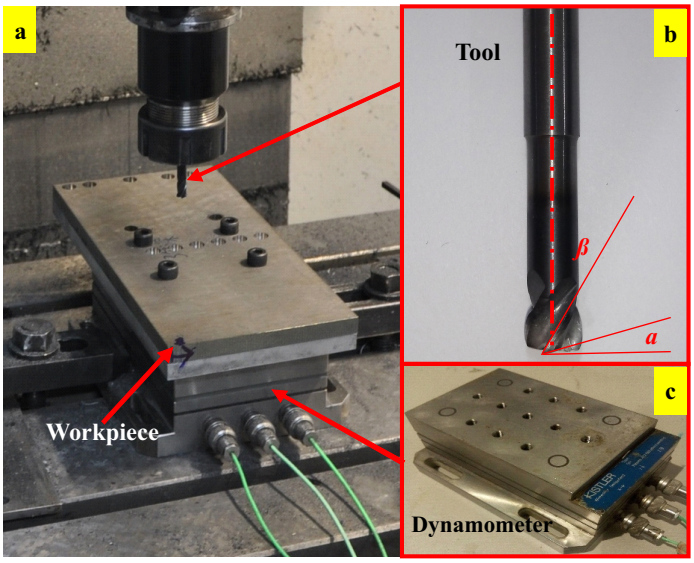

Fig. 6 Experimental setup for the measure of cutting forces

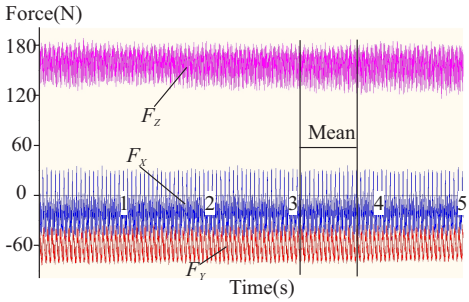

Fig. 7 Measured cutting force in slot milling

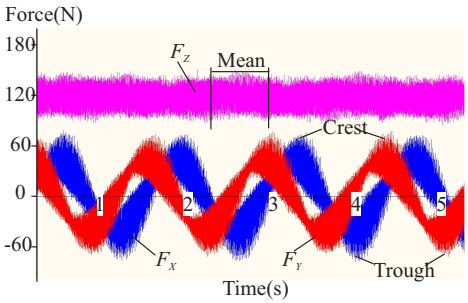

Fig. 8 Measured cutting force in helical milling hole-making

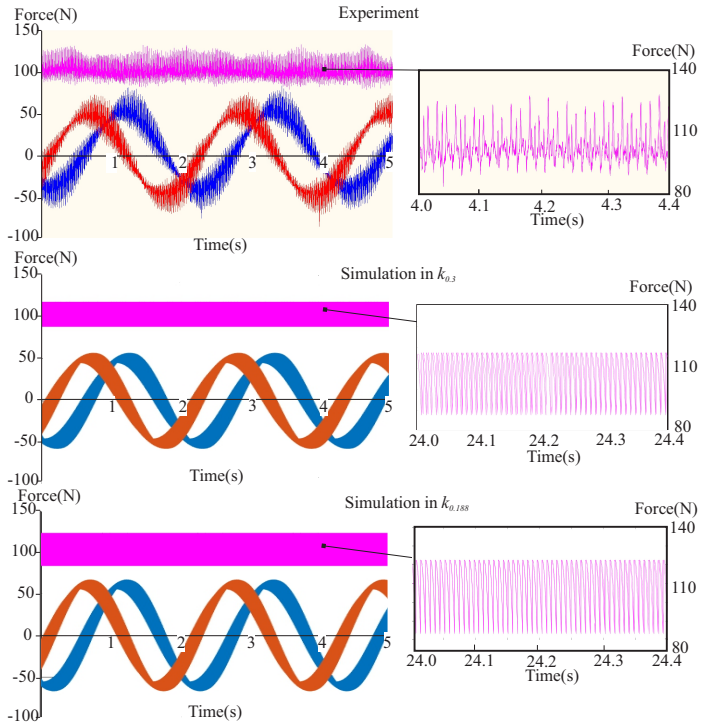

Fig. 9 The experimental results comparing with the simulation results(s_t = 0.045mm/tooth, n = 2000 rpm, a_p = 0.3mm)

Table 1 The parameters of cutting tool

Parameters	Content
Diameter (D_t)	6 mm
Rake angle (β)	30 deg
Relief angle (α)	10 deg
Number of teeth (N)	4
Nose radius (R_n)	0.05 mm

Table 2 Chemical composition of Ti6Al4V alloy

Element	C	Fe	N	O	Al	V	Ti
Content (Wt.%)	< 0.08	< 0.25	< 0.05	0.2	5.5-6.76	3.5-4.5	Balance

Table 3 Basic mechanical properties of Ti6Al4V specimen

Parameters	Content
Tensile strength	950 MPa
Elongation	8%
Density	4430 kg/m^3
Youngs modulus	113 GPa
Poissons ratio	0.342

Table 4 The cutting conditions at spindle speed = 2000 rpm

No.	Slotting b(mm)	s_t (mm/tooth)	No.	Slotting b(mm)	s_t (mm/tooth)	No.	Helical Milling a_p(mm/rev)	s_t (mm/tooth)
1	0.188	0.02	7	0.3	0.02	13	0.3	0.02
2	0.188	0.025	8	0.3	0.025	14	0.3	0.025
3	0.188	0.03	9	0.3	0.03	15	0.3	0.03
4	0.188	0.035	10	0.3	0.035	16	0.3	0.035
5	0.188	0.04	11	0.3	0.04	17	0.3	0.04
6	0.188	0.045	12	0.3	0.045	18	0.3	0.045

Table 5 Helical milling experiments at different a_p

No.	a_p mm/rev	s_t mm/tooth	n rpm
19	0.15	0.035	2000
20	0.2	0.035	2000
21	0.25	0.035	2000
22	0.3	0.035	2000
23	0.35	0.035	2000

Table 6 The cutting force coefficients calibrated in different b

Coefficient name	k_{Pr}	k_{Pre}	k_{Pt}	k_{Pte}	k_{Pa}	k_{Pae}	k_{Fa}	k_{Fae}
$k_{0.188}$ N/mm^2	292	10.5	3360	55.6	1810	132.6	279	3
$k_{0.3}$ N/mm^2	315	15.6	2340	58.9	1100	100	740	4

Table 7 The experiment and simulation cutting forces

Cutting force type		EXP		$k_{0.188}$		$k_{0.3}$	
No.	s_t (mm/tooth)	$\overline{F}_{hxy}$ (N)	$\overline{F}_{hz}$ (N)	$\overline{F}_{hxy}$ (N)	$\overline{F}_{hz}$ (N)	$\overline{F}_{hxy}$ (N)	$\overline{F}_{hz}$ (N)
13	0.02	51	93	52.7	91.5	47.8	93
14	0.025	57	96.4	55.2	93	49.5	95
15	0.03	61.5	98.79	58	95	51.2	97.5
16	0.035	66	99.4	60.8	97.5	53	98.1
17	0.04	68	100.5	64	101	54.9	100.2
18	0.045	70.5	105	66.8	105	57	102.1

Table 8 The error between simulation and experimental results

s_t (mm/tooth)	$k_{0.188}$		$k_{0.3}$	
	R_{hxy} (%)	R_{hz} (%)	R_{hxy} (%)	R_{hz} (%)
0.02	-3.33	1.61	6.27	0
0.025	3.16	3.53	13.16	1.45
0.03	5.69	3.84	16.75	1.31
0.035	7.89	1.91	19.7	1.31
0.04	5.88	-0.5	19.26	0.3
0.045	5.25	0	19.15	2.7
Mean Error	4.08	1.73	15.72	1.19

Table 9 Relation of depth of cut a_p and cutting forces

Cutting force type			EXP		$k_{0.188}$		Error	
No.	a_p (mm/rev)	$\overline{b}$ (mm)	$\overline{F}_{hxy}$ (N)	$\overline{F}_{hz}$ (N)	$\overline{F}_{hxy}$ (N)	$\overline{F}_{hz}$ (N)	R_{hxy} (%)	R_{hz} (%)
19	0.15	0.094	51	93	52.7	91.5	40.4	15.6
20	0.2	0.13	57	96.4	55.2	93	31.3	12.1
21	0.25	0.16	61.5	98.79	58	95	22.7	12.2
22	0.3	0.188	66	99.4	60.8	97.5	7.9	1.9
23	0.35	0.22	70.5	105	66.8	105	-4.6	-5.5